Modal parameter identification based on ARMAV and state–space approaches

Joseph Lardies

Modal parameter identification based on ARMAV and state–space approaches

Joseph Lardies

Abstract An accurate prediction for the response of civil and mechanical engineering structures subject to ambient excitation requires the information of dynamic properties of these structures including natural frequencies, damping ratios and mode shapes. Since the excitation force is not available as a measured signal, we need to develop techniques which are capable of accurately extracting the modal parameters from output-only data. This article presents the results of modal parameter identification using two time-domain methods as follows: the autoregressive moving average vector (ARMAV) method and the state–space method. These methods directly work with the recorded time signals and allow the analysis of structures where only the output is measured, while the input is unmeasured and unknown. The equivalence between ARMAV and state–space approaches for the problem of modal parameter identification of vibrating systems is shown in the article. Using only the singular value decomposition of a block Hankel matrix of sample covariances, it is shown that these two approaches give identical modal parameters in the case where the block Hankel matrix has full row rank. The time-domain modal identification algorithms have a serious problem of model order determination: when extracting structural modes these algorithms always generate spurious modes. A modal indicator to differentiate spurious and structural modes is presented. Numerical and experimental examples are given to show the effectiveness of the ARMAV or state–space approaches in modal parameter identification using response data only.

Keywords System identification · Time domain · State–space · Ambient excitation · Transition matrix · Companion matrix

1 Introduction

System identification has been originally developed in control engineering [1] and has been received a worldwide attention for various types of applications [2–5]. In the context of civil and mechanical engineering structures, such as bridges, buildings, towers, off-shore platforms, turbines, aircraft prototypes, and so on, the system identification procedure means the extraction of modal parameters such as eigenfrequencies, damping ratios and mode shapes. These modal parameters can serve as reference or input to model updating in the finite element modeling of structures; they can be utilized for structural control and damage detection. Traditionally, the modal parameter identification is carried out based on both input and output measurement data through the frequency-response functions in the frequency domain and impulse-response function in the time domain. For civil and mechanical engineering systems, the dynamic responses or outputs are the time records of the sensors that are installed at several locations. However, in operational conditions the input or excitation of the structure is unknown and cannot be quantified and used in the identification procedure. It is impossible

J. Lardies (✉)
Department of Applied Mechanics, L.M.A.R.C., Institute FEMTO-ST, UMR CNRS 6174,
University of Franche-Comté, 25 000 Besançon, France
E-mail: joseph.lardies@univ-fcomte.fr

to measure this ambient excitation, and the outputs are the only information that can be used in the system identification algorithms. It is assumed that the input is a stochastic process (a white noise) and we have then a stochastic system identification process. Note that if the white noise assumption is not verified, for instance, if the input contains in addition to white noise also some frequency components, these frequencies cannot be separated from the eigenfrequencies of the analyzed structure and will be identified as such.

It is obvious that real operating conditions of complex structures may significantly differ from those of controlled laboratory environments, and due to this reason, the need to identify modal parameters under real operational conditions is primordial. Operational modal analysis, also called natural-excitation or output-only modal analysis, utilizes only response measurements of structures at work and has many advantages: it is easy to use, fast to conduct and inexpensive since no artificial excitation equipment is needed to excite the structure. Furthermore, no boundary condition simulation is required, the identification of modal properties of the whole system at representative working points can be obtained, and finally, operational modal analysis can not only be utilized for structural dynamics analysis and design but also for vibration control and structural health monitoring. Note that in experimental tests in laboratory, where artificial excitations such as a swept sine, periodic chirp, impact or random forces are applied, output-only modal analysis techniques can also be applied. The modal parameter identification technique through operational modal analysis has become a very attractive topic in the area of civil and mechanical engineering structures and several algorithms have been proposed in the literature. These algorithms work in the frequency domain, in the time domain or in the time–frequency domain. In the frequency domain [5], the power spectral density of output responses is obtained using several signal processing techniques and natural frequencies are determined through a peak-picking procedure. It is proposed in [6] a frequency domain procedure to obtain damping ratios of building structures under seismic excitations. However, in general, there are limits with these methods in dealing with heavy damping and closeness of natural frequencies. The reason for the limitation is essentially modal interference and hence some individual modes and natural frequencies cannot be observed individually. In the time domain [7–10] correlation functions or covariance matrices between output responses are used to obtain a companion matrix or a transition matrix and extract modal parameters from eigen decomposition of these matrices. In the time–frequency domain [11,12] the wavelet transform of the free response of the structure is used. The wavelet transform of a signal results in a complex valued form and it is shown that the modulus of the wavelet transform is related to damping ratios and its phase to eigenfrequencies. The identification procedure using the wavelet transform requires the free response of signals, however, in operational modal analysis the measured signals are random. The ambient data are then transformed into free vibration data, before usage of the wavelet transform, by the application of the random decrement technique [13].

We propose in this work two time-domain procedures to extract the modal parameters of vibrating systems from output-only measurements: the autoregressive moving average vector (ARMAV) approach and the state–space approach based on the stochastic realization algorithm. These two approaches have been applied to estimate the modal parameters of structures in real operational conditions [8,14–20]. With the ARMAV approach, the modal parameters are extracted by solving a standard eigendecomposition problem of the companion matrix containing the AR coefficients. With the state–space approach the modal parameters are obtained by solving a standard eigendecomposition problem of the discrete state matrix, or transition matrix. In this article, we describe briefly these two approaches and establish the relationship between the companion matrix and the discrete state matrix. It is shown that these two approaches give the same eigenvalues, and thus the same modal parameters, in the cases where the block Hankel matrix of covariances has full row rank. A generalized weighted concept of the ARMAV and state–space approaches is also analyzed and the relationship between the eigenvectors of the discrete state matrix and the eigenvectors of the companion matrix is established.

This article is organized as follows. In Sect. 2, the ARMAV approach and the companion matrix, which contain the basic information about the vibrating structure are presented. In Sect. 3, the state–space approach and the discrete state matrix (or transition matrix) containing all modal information are derived. It is shown in Sect. 4 that the companion matrix and the discrete state matrix are related by a similarity transformation, which implies that they have the same eigenvalues. We obtain then the same eigenfrequencies and damping ratios of a vibrating system with the ARMAV approach and with the state–space approach. The relation between the eigenvectors, which give the mode shapes of the structure, using the ARMAV and state–space approaches is also formulated. The modal parameter identification algorithms have a serious problem of model order determination: when extracting physical or structural modes, these algorithms always generate spurious or computational modes. A criterion based on the modal coherence of measured and identified modes is used to detect these spurious modes and remove them from the model. This algorithm is described in Sect. 5. In Sect. 6,

simulation results and experimental results in laboratory and in environmental conditions are presented. This article is briefly concluded in Sect. 7.

2 The ARMAV model

The mixed ARMAV model can be used to represent the dynamics of a mechanical system [3,19–21]. It is shown that the difference equation for an ARMAV time series is

$$\mathbf{y}_{k+f} - \sum_{j=1}^{f} \boldsymbol{\alpha}_j \mathbf{y}_{k+f-j} = \sum_{j=1}^{f} \boldsymbol{\beta}_j \mathbf{e}_{k+f-j} \tag{1}$$

The left side of this equation is the vector autoregressive (AR) part and the right side is the vector moving average (MA) part. The AR part describes the system dynamics and contains all the modal information of the vibrating system while the MA part is related to the external noise as well to the excitation. If m is the number of sensors, $\mathbf{y}_k$ is an $(m \times 1)$ vector of observations at time $k : \mathbf{y}_k = [y_{1k}, y_{2k}, \ldots, y_{mk}]^{\mathrm{T}}$, where the superscript T denotes the transpose. Also, $\mathbf{e}_k$ is an $(m \times 1)$ zero-mean vector white noise process, $\boldsymbol{\alpha}_j$'s are the AR parameter matrices $(m \times m)$ and $\boldsymbol{\beta}_j$'s are the MA parameter matrices $(m \times m)$. The multi-dimensional ARMAV representation (Eq. 1) can be expressed as

$$\begin{bmatrix} \mathbf{y}_{k+1} \\ \mathbf{y}_{k+2} \\ . \\ . \\ \mathbf{y}_{k+f} \end{bmatrix} = \begin{bmatrix} \mathbf{0} & \mathbf{I} & \mathbf{0} & . & \mathbf{0} \\ \mathbf{0} & \mathbf{0} & \mathbf{I} & . & \mathbf{0} \\ . & . & . & . & . \\ \mathbf{0} & \mathbf{0} & \mathbf{0} & . & \mathbf{I} \\ \boldsymbol{\alpha}_f & \boldsymbol{\alpha}_{f-1} & . & . & \boldsymbol{\alpha}_1 \end{bmatrix} \begin{bmatrix} \mathbf{y}_k \\ \mathbf{y}_{k+1} \\ . \\ . \\ \mathbf{y}_{k+f-1} \end{bmatrix} + \begin{bmatrix} \mathbf{0} & \mathbf{0} & \mathbf{0} & . & \mathbf{0} \\ \mathbf{0} & \mathbf{0} & \mathbf{0} & . & \mathbf{0} \\ . & . & . & . & . \\ \mathbf{0} & \mathbf{0} & \mathbf{0} & . & \mathbf{0} \\ \boldsymbol{\beta}_f & \boldsymbol{\beta}_{f-1} & . & . & \boldsymbol{\beta}_1 \end{bmatrix} \begin{bmatrix} \mathbf{e}_k \\ \mathbf{e}_{k+1} \\ . \\ . \\ \mathbf{e}_{k+f-1} \end{bmatrix} \tag{2}$$

Only the AR parameter matrices are necessary in order to identify the modal parameters of the vibrating system [3,21]. These AR coefficients form the $(mf \times mf)$ companion matrix $\boldsymbol{\alpha}$ defined as

$$\boldsymbol{\alpha} = \begin{bmatrix} \mathbf{0} & \mathbf{I} & \mathbf{0} & . & \mathbf{0} \\ \mathbf{0} & \mathbf{0} & \mathbf{I} & . & \mathbf{0} \\ . & . & . & . & . \\ \mathbf{0} & \mathbf{0} & \mathbf{0} & . & \mathbf{I} \\ \boldsymbol{\alpha}_f & \boldsymbol{\alpha}_{f-1} & . & . & \boldsymbol{\alpha}_1 \end{bmatrix} \tag{3}$$

and our objective is to find this companion matrix that can be eigenvalue-eigenvector decomposed. The eigenvalues are related to natural frequencies and damping ratios of the structure and the eigenvectors are related to the mode shapes.

Define the $(mf \times 1)$ and $(mp \times 1)$ future and past data vectors as $\mathbf{y}_k^+ = \left[\mathbf{y}_k^{\mathrm{T}}, \mathbf{y}_{k+1}^{\mathrm{T}}, \ldots, \mathbf{y}_{k+f-1}^{\mathrm{T}}\right]^{\mathrm{T}}$ and $\mathbf{y}_k^- = \left[\mathbf{y}_k^{\mathrm{T}}, \mathbf{y}_{k-1}^{\mathrm{T}}, \ldots, \mathbf{y}_{k-p+1}^{\mathrm{T}}\right]^{\mathrm{T}}$. Define also the $(mf \times 1)$ vector $\mathbf{e}_k^+$ as $\mathbf{e}_k^+ = \left[\mathbf{e}_k^{\mathrm{T}}, \mathbf{e}_{k+1}^{\mathrm{T}}, \ldots, \mathbf{e}_{k+f-1}^{\mathrm{T}}\right]^{\mathrm{T}}$ and the $(mf \times mf)$ matrix $\boldsymbol{\beta}$ as

$$\boldsymbol{\beta} = \begin{bmatrix} \mathbf{0} & \mathbf{0} & \mathbf{0} & . & \mathbf{0} \\ \mathbf{0} & \mathbf{0} & \mathbf{0} & . & \mathbf{0} \\ . & . & . & . & . \\ \mathbf{0} & \mathbf{0} & \mathbf{0} & . & \mathbf{0} \\ \boldsymbol{\beta}_f & \boldsymbol{\beta}_{f-1} & . & . & \boldsymbol{\beta}_1 \end{bmatrix} \tag{4}$$

Equation (2) is then expressed as

$$\mathbf{y}_{k+1}^+ = \boldsymbol{\alpha}\mathbf{y}_k^+ + \boldsymbol{\beta}\mathbf{e}_k^+ \tag{5}$$

Multiplying Eq. (5) by the $(1 \times mp)$ vector $\mathbf{y}_{k-1}^{-\mathrm{T}}$ and taking expectation of the multiplication result we obtain

$$E\left[\mathbf{y}_{k+1}^+ \mathbf{y}_{k-1}^{-\mathrm{T}}\right] = \boldsymbol{\alpha} E\left[\mathbf{y}_k^+ \mathbf{y}_{k-1}^{-\mathrm{T}}\right] + \boldsymbol{\beta} E\left[\mathbf{e}_k^+ \mathbf{y}_{k-1}^{-\mathrm{T}}\right] \tag{6}$$

We define the $(mf \times mp)$ block Hankel matrix $\mathbf{H}$ and the $(mf \times mp)$ time shifted block Hankel matrix $\overleftarrow{\mathbf{H}}$ as

$$\mathbf{H} = E\left[\mathbf{y}_k^+ \quad \mathbf{y}_{k-1}^{-T}\right] = \begin{bmatrix} \mathbf{R}_1 & \mathbf{R}_2 & . & \mathbf{R}_p \\ \mathbf{R}_2 & \mathbf{R}_3 & . & \mathbf{R}_{p+1} \\ . & . & . & . \\ \mathbf{R}_f & \mathbf{R}_{f+1} & . & \mathbf{R}_{f+p-1} \end{bmatrix}; \quad \overleftarrow{\mathbf{H}} = E\left[\mathbf{y}_{k+1}^+ \quad \mathbf{y}_{k-1}^{-T}\right] = \begin{bmatrix} \mathbf{R}_2 & \mathbf{R}_3 & . & \mathbf{R}_{p+1} \\ \mathbf{R}_3 & \mathbf{R}_4 & . & \mathbf{R}_{p+2} \\ . & . & . & . \\ \mathbf{R}_{f+1} & \mathbf{R}_{f+2} & . & \mathbf{R}_{f+p} \end{bmatrix} \tag{7}$$

where $\{\mathbf{R}_i\}$ are the $(m \times m)$ theoretical covariance matrices of observed time series $\mathbf{y}_k$: $\mathbf{R}_i = E[\mathbf{y}_k \quad \mathbf{y}_{k-i}^{\mathrm{T}}]$. The left arrow notation is motivated by interpreting $\overleftarrow{\mathbf{H}}$ as a block Hankel matrix with the blocks of $\mathbf{H}$ shifted left one position and then the last column filled on the right. Because $\mathbf{e}_k^+$ is uncorrelated with $\mathbf{y}_{k-1}^-$ we have $E[\mathbf{e}_k^+ \quad \mathbf{y}_{k-1}^{-T}] = \mathbf{0}$ and Eq. (6) becomes

$$\overleftarrow{\mathbf{H}} = \boldsymbol{\alpha}\mathbf{H} \tag{8}$$

Under the assumption that the block Hankel matrix of covariances has full row rank, the companion matrix $\boldsymbol{\alpha}$ is uniquely given by

$$\boldsymbol{\alpha} = \overleftarrow{\mathbf{H}}\mathbf{H}^{\mathrm{T}}\left(\mathbf{H}\mathbf{H}^{\mathrm{T}}\right)^{-1} \tag{9}$$

Let

$$\mathbf{H} = \mathbf{U}\boldsymbol{\Sigma}\mathbf{V}^{\mathrm{T}} \tag{10}$$

denote the singular value decomposition (SVD) [2,9,22–24] of the matrix $\mathbf{H}$, $\boldsymbol{\Sigma}$ is a diagonal matrix of singular values and $\mathbf{U}$ and $\mathbf{V}$ are matrices of appropriate dimensions which satisfy $\mathbf{U}^{\mathrm{T}}\mathbf{U} = \mathbf{I}$ and $\mathbf{V}^{\mathrm{T}}\mathbf{V} = \mathbf{I}$. In this paper, it is assumed that rank $(\mathbf{H}) = mf$. Under this assumption the diagonal matrix $\boldsymbol{\Sigma}$ has dimension $(mf \times mf)$ and $\mathbf{U}$ and $\mathbf{V}$ have dimensions $(mf \times mf)$ and $(mp \times mf)$ respectively. Hence, $\mathbf{U}$ is an orthogonal matrix and $\mathbf{V}$ is a semi-orthogonal matrix. It should be noted that the assumption rank$(\mathbf{H}) = mf$ essentially means that $p \geq f$ and that we want to determine $mf/2$ pairs of complex conjugate eigenvalues from the companion matrix $\boldsymbol{\alpha}$ and consequently $mf/2$ modal parameters. This rank condition is not necessary related to the assumption that mf is the true order of the process $\{\mathbf{y}_k\}$, because for $p \geq f$ the matrix $\mathbf{H}$ has full row rank even if the process $\{\mathbf{y}_k\}$ is of lower order than mf. The condition $p \geq f$ is a natural condition because the statistical accuracy of the modal parameter estimates may increase significantly with increasing p (or mp). It is well known that much more accurate modal parameter estimates are obtained with the overdetermined equations (8) (with $p >> f$) than with the exactly determined equations (8) (with $p = f$).

Inserting the SVD of $\mathbf{H}$ in Eq. (9), we obtain

$$\boldsymbol{\alpha} = \overleftarrow{\mathbf{H}}\mathbf{V}\boldsymbol{\Sigma}\mathbf{U}^{\mathrm{T}}\left(\mathbf{U}\boldsymbol{\Sigma}^2\mathbf{U}^{\mathrm{T}}\right)^{-1} = \overleftarrow{\mathbf{H}}\mathbf{V}\boldsymbol{\Sigma}^{-1}\mathbf{U}^{\mathrm{T}} \tag{11}$$

The companion matrix can be obtained by the singular value decomposition of the block Hankel matrix $\mathbf{H}$ and the use of a shifted block Hankel matrix.

3 The state–space model

For a linear vibrating system with viscous damping the equation of motion can be transformed into a discrete time stochastic state–space model [2,4,7–10,16–18]

$$\mathbf{z}_{k+1} = \mathbf{A}\mathbf{z}_k + \mathbf{u}_k \tag{12}$$

$$\mathbf{y}_k = \mathbf{C}\mathbf{z}_k + \mathbf{v}_k \tag{13}$$

where $\mathbf{z}_k$ is the $(mf \times 1)$ discrete time state vector; $\mathbf{A}$ is the $(mf \times mf)$ discrete state matrix (or transition matrix) containing all modal information; $\mathbf{C}$ is the (m × mf) output matrix ; $\mathbf{u}_k$ corresponds to the excitation vector and

$\mathbf{v}_k$ is the measurement noise vector. It is assumed that $\mathbf{u}_k$ and $\mathbf{v}_k$ are zero mean white noise sequences, independent of the current state $\mathbf{z}_k$, so that $E[\mathbf{u}_k] = \mathbf{0}$; $E[\mathbf{v}_k] = \mathbf{0}$; $E[\mathbf{z}_k\mathbf{u}_k^{\mathrm{T}}] = \mathbf{0}$; $E[\mathbf{z}_k\mathbf{v}_k^{\mathrm{T}}] = \mathbf{0}$; $E[\mathbf{u}_{k+i}\mathbf{u}_k^{\mathrm{T}}] = 0$ for $i \neq \mathbf{0}$; $E[\mathbf{v}_{k+i}\mathbf{v}_k^{\mathrm{T}}] = \mathbf{0}$ for $i \neq \mathbf{0}$. The output covariance matrices are [1–5,23]

$$\mathbf{R}_i = E[\mathbf{y}_k \;\; \mathbf{y}_{k-i}^{\mathrm{T}}] = \mathbf{C}\mathbf{A}^{i-1}\mathbf{G} \tag{14}$$

where $\mathbf{G} = E[\mathbf{z}_{k+1}\mathbf{y}_k^{\mathrm{T}}]$. The block Hankel matrix of covariances is factorized into its observability and controllability matrices, $\mathbf{O}$ $(mf \times mf)$ and $\mathbf{K}$ $(mf \times mp)$ [2,22–24]

$$\mathbf{H} = E\left[\mathbf{y}_k^{+}\mathbf{y}_{k-1}^{-T}\right] = \begin{bmatrix} \mathbf{C} \\ \mathbf{C}\mathbf{A} \\ . \\ \mathbf{C}\mathbf{A}^{f-1} \end{bmatrix} [\mathbf{G} \quad \mathbf{A}\mathbf{G} \quad \mathbf{A}^2\mathbf{G}, \ldots, \mathbf{A}^{p-1}\mathbf{G}] = \mathbf{O}\mathbf{K} \tag{15}$$

The aforementioned rank properties of the block Hankel matrix $\mathbf{H}$ together with Eq. (15) imply that the observability matrix has full column rank and that the controllability matrix has full row rank. The two factorizations of the block Hankel matrix given by Eqs. (10) and (15) are equated to give

$$\mathbf{H} = (\mathbf{U}\boldsymbol{\Sigma}^{1/2})(\boldsymbol{\Sigma}^{1/2}\mathbf{V}^{\mathrm{T}}) = \mathbf{O}\mathbf{K} \tag{16}$$

where $\boldsymbol{\Sigma}^{1/2}$ is the square root of $\boldsymbol{\Sigma}$. Note that

$$\mathbf{O} = \mathbf{U}\boldsymbol{\Sigma}^{1/2}; \quad \mathbf{K} = \boldsymbol{\Sigma}^{1/2}\mathbf{V}^{\mathrm{T}} \tag{17}$$

and the generalized inverses of $\mathbf{O}$ and $\mathbf{K}$ are

$$\mathbf{O}^{+} = \boldsymbol{\Sigma}^{-1/2}\mathbf{U}^{\mathrm{T}}; \quad \mathbf{K}^{+} = \mathbf{V}\boldsymbol{\Sigma}^{-1/2} \tag{18}$$

To determine the discrete state matrix $\mathbf{A}$, it is necessary to introduce the shifted block Hankel matrix

$$\overleftarrow{\mathbf{H}} = E\left[\mathbf{y}_{k+1}^{+}\mathbf{y}_{k-1}^{-T}\right] = \mathbf{O}\mathbf{A}\mathbf{K} \tag{19}$$

The matrix $\mathbf{A}$ is obtained by applying the generalized inverses of $\mathbf{O}$ and $\mathbf{K}$, yielding

$$\mathbf{A} = \mathbf{O}^{+}\overleftarrow{\mathbf{H}}\mathbf{K}^{+} = \boldsymbol{\Sigma}^{-1/2}\mathbf{U}^{\mathrm{T}}\overleftarrow{\mathbf{H}}\mathbf{V}\boldsymbol{\Sigma}^{-1/2} \tag{20}$$

In the next section we establish a simple relation between the companion matrix $\boldsymbol{\alpha}$ and the discrete state matrix $\mathbf{A}$.

4 Equivalence between state–space and ARMAV approaches in modal analysis

Using the property $\mathbf{U}^{\mathrm{T}}\mathbf{U} = \mathbf{I}$, we can write Eq. (20) as

$$\mathbf{A} = \boldsymbol{\Sigma}^{-1/2}\mathbf{U}^{\mathrm{T}}\overleftarrow{\mathbf{H}}\mathbf{V}\boldsymbol{\Sigma}^{-1}\mathbf{U}^{\mathrm{T}}\mathbf{U}\boldsymbol{\Sigma}^{1/2} \tag{21}$$

and inserting the value of the companion matrix (11), we obtain

$$\mathbf{A} = \boldsymbol{\Sigma}^{-1/2}\mathbf{U}^{\mathrm{T}}\boldsymbol{\alpha}\mathbf{U}\boldsymbol{\Sigma}^{1/2} \tag{22}$$

Thus, matrices $\mathbf{A}$ and $\boldsymbol{\alpha}$ are related by a similarity transformation, which implies that they have the same eigenvalues. In the cases where the block Hankel matrix of covariances has full row rank, the modal parameters obtained by the companion matrix or by the discrete state matrix are the same.

It also seems natural to define a generalized weighted concept by introducing an $(mp \times mp)$ weighting matrix $\mathbf{W}$. Some weighting matrices can be obtained in [9,23] based on canonical variate analysis and balanced realization approaches. So, instead of Eq. (8) we, consider

$$\overleftarrow{\mathbf{H}}\mathbf{W} = \boldsymbol{\alpha}\mathbf{H}\mathbf{W} \Rightarrow \boldsymbol{\alpha} = \overleftarrow{\mathbf{H}}\mathbf{W}(\mathbf{H}\mathbf{W})^{\mathrm{T}}[(\mathbf{H}\mathbf{W})(\mathbf{H}\mathbf{W})^{\mathrm{T}}]^{-1} \tag{23}$$

under the assumption that the product (**HW**) has full row rank. The singular value decomposition of the product (bf HW) is

$$\mathbf{HW} = \breve{\mathbf{U}}\breve{\mathbf{\Sigma}}\breve{\mathbf{V}}^{\mathrm{T}} \tag{24}$$

Inserting this singular value decomposition in Eq. (23), we obtain the companion matrix

$$\boldsymbol{\alpha} = \overleftarrow{\mathbf{H}}\mathbf{W}\breve{\mathbf{V}}\breve{\mathbf{\Sigma}}^{-1}\breve{\mathbf{U}}^{\mathrm{T}} \tag{25}$$

In the weighted coordinate system, the discrete state–space approach becomes

$$\mathbf{OKW} = \breve{\mathbf{U}}\breve{\mathbf{\Sigma}}^{1/2}\breve{\mathbf{\Sigma}}^{1/2}\breve{\mathbf{V}}^{\mathrm{T}} \tag{26}$$

and the generalized inverses of the observability and controllability matrices are

$$\mathbf{O}^{+} = \breve{\mathbf{\Sigma}}^{-1/2}\breve{\mathbf{U}}^{\mathrm{T}} \;; \quad \mathbf{K}^{+} = \mathbf{W}\breve{\mathbf{V}}\breve{\mathbf{\Sigma}}^{-1/2} \tag{27}$$

The discrete state matrix is then given by

$$\mathbf{A} = \breve{\mathbf{\Sigma}}^{-1/2}\breve{\mathbf{U}}^{\mathrm{T}}\overleftarrow{\mathbf{H}}\mathbf{W}\breve{\mathbf{V}}\breve{\mathbf{\Sigma}}^{-1/2} = \breve{\mathbf{\Sigma}}^{-1/2}\breve{\mathbf{U}}^{\mathrm{T}}\overleftarrow{\mathbf{H}}\mathbf{W}\breve{\mathbf{V}}\breve{\mathbf{\Sigma}}^{-1}\breve{\mathbf{U}}^{\mathrm{T}}\breve{\mathbf{U}}\breve{\mathbf{\Sigma}}^{1/2} \tag{28}$$

$$\mathbf{A} = \breve{\mathbf{\Sigma}}^{-1/2}\breve{\mathbf{U}}^{\mathrm{T}}\boldsymbol{\alpha}\breve{\mathbf{U}}\breve{\mathbf{\Sigma}}^{1/2} \tag{29}$$

Thus, matrices **A** and $\boldsymbol{\alpha}$ are again related by a similarity transformation, which implies that they have the same eigenvalues.

Thus, matrices **A** and $\boldsymbol{\alpha}$ are again related by a similarity transformation, which implies that they have the same eigenvalues.

Now, we can determine the relation between the eigenvectors of the discrete state matrix **A** and the eigenvectors of the companion matrix $\boldsymbol{\alpha}$. Let $\mathbf{\Lambda}$ be the diagonal matrix of eigenvalues, $\mathbf{\Psi}$ and $\mathbf{\Phi}$ the eigenvectors matrices of **A** and $\boldsymbol{\alpha}$, respectively. We have from Eq. (21), or from Eq. (29)

$$\mathbf{A}\mathbf{\Sigma}^{-1/2}\mathbf{U}^{\mathrm{T}} = \mathbf{\Sigma}^{-1/2}\mathbf{U}^{\mathrm{T}}\boldsymbol{\alpha} \tag{30}$$

$$\mathbf{A}\mathbf{\Sigma}^{-1/2}\mathbf{U}^{\mathrm{T}} = \mathbf{\Sigma}^{-1/2}\mathbf{U}^{\mathrm{T}}\mathbf{\Phi}\mathbf{\Lambda}\mathbf{\Phi}^{-1} \tag{31}$$

$$\mathbf{A}\mathbf{\Sigma}^{-1/2}\mathbf{U}^{\mathrm{T}}\mathbf{\Phi} = \mathbf{\Sigma}^{-1/2}\mathbf{U}^{\mathrm{T}}\mathbf{\Phi}\mathbf{\Lambda} \tag{32}$$

$$\mathbf{A}\mathbf{\Psi} = \mathbf{\Psi}\mathbf{\Lambda} \tag{33}$$

As we can see, the relation between the eigenvectors matrices of **A** and $\boldsymbol{\alpha}$ is

$$\mathbf{\Psi} = \mathbf{\Sigma}^{-1/2}\mathbf{U}^{\mathrm{T}}\mathbf{\Phi} \tag{34}$$

and these eigenvectors are related to the modal vectors or mode shapes of the mechanical structure.

5 Modal parameter identification procedure

We have shown that the ARMAV and state–space methods give the same modal parameters. In the following we consider only the state–space approach. The modal parameters of a vibrating structure are obtained by applying the eigenvalue decomposition of the discrete state matrix **A**

$$\mathbf{A} = \mathbf{\Psi}\mathbf{\Lambda}\mathbf{\Psi}^{-1} \tag{35}$$

where $\mathbf{\Lambda} = \mathrm{dig}(\lambda_i), \quad i = 1, 2, \ldots, n,$ is the diagonal matrix containing the complex eigenvalues and $\mathbf{\Psi}$ contains the eigenvectors of **A** as columns. The eigenfrequencies f_i and damping ratios ζ_i are related to the eigenvalues λc_i of the corresponding continuous-time system [2–5]:

$$\lambda c_i = \frac{\log(\lambda_i)}{\Delta t} = -2\pi f_i \zeta_i \pm j 2\pi f_i \sqrt{1-\zeta_i^2} \tag{36}$$

$$f_i = \frac{|\lambda c_i|}{2\pi}; \quad \zeta_i = \frac{-\mathrm{Re}(\lambda c_i)}{2\pi f_i} \tag{37}$$

where $|\lambda c_i|$ and $\mathrm{Re}(\lambda c_i)$ denote the modulus and the real part of the complex number λc_i and Δt the sampling period of analyzed signals. The mode shapes are evaluated at the sensor locations by multiplying the output matrix $\mathbf{C}$ with the matrix of eigenvectors.

However, all the state–space methods have a serious problem of model order determination. When extracting physical or structural modes these methods always generate spurious or computational modes to account for unwanted effects such as noise, leakage, residuals, nonlinearity's … Furthermore, weakly excited modes often require relatively high numbers of assumed modes to be properly identified. For these reasons, the assumed number of modes, or model order, is incremented over a wide range of values and we plot the stability diagram. The stability diagram involves tracking the estimates of eigenfrequencies and damping ratios as a function of model order. As the model order is increased, more and more modal frequencies and damping ratios are estimated, hopefully, the estimates of the physical modal parameters stabilize as the correct model order is reached. For modes which are very active in the measured data, the modal parameters stabilize at a very low model order. For modes poorly excited, the modal parameters may not stabilize until a very high model order is chosen. Nevertheless, the non-physical modes, called spurious modes, do not stabilize at all during this process and can be sorted out of the modal parameters. A criterion based on the modal coherence of measured and identified modes is used to detect these spurious modes and remove them from the model.

In first we define the modal observability coherence indicator. In modal coordinates the identified covariance matrices are

$$\mathbf{R}_i = \widetilde{\mathbf{C}}\boldsymbol{\Lambda}^{i-1}\widetilde{\mathbf{G}} \tag{38}$$

where $\widetilde{\mathbf{C}} = \mathbf{C}\boldsymbol{\Psi}$ is the identified matrix of mode shapes or output matrix in modal coordinates and $\widetilde{\mathbf{G}} = \boldsymbol{\Psi}^{-1}\mathbf{G}$ the identified cross-covariance matrix between the state and the output. In modal coordinates the block Hankel matrix is

$$\mathbf{H} = \begin{bmatrix} \widetilde{\mathbf{C}}\widetilde{\mathbf{G}} & \widetilde{\mathbf{C}}\boldsymbol{\Lambda}\widetilde{\mathbf{G}} & . & \widetilde{\mathbf{C}}\boldsymbol{\Lambda}^{p-1}\widetilde{\mathbf{G}} \\ \widetilde{\mathbf{C}}\boldsymbol{\Lambda}\widetilde{\mathbf{G}} & \widetilde{\mathbf{C}}\boldsymbol{\Lambda}^{2}\widetilde{\mathbf{G}} & . & \widetilde{\mathbf{C}}\boldsymbol{\Lambda}^{p}\widetilde{\mathbf{G}} \\ . & . & . & . \\ \widetilde{\mathbf{C}}\boldsymbol{\Lambda}^{f-1}\widetilde{\mathbf{G}} & \widetilde{\mathbf{C}}\boldsymbol{\Lambda}^{f}\widetilde{\mathbf{G}} & . & \widetilde{\mathbf{C}}\boldsymbol{\Lambda}^{f+p-2}\widetilde{\mathbf{G}} \end{bmatrix} = \begin{bmatrix} \widetilde{\mathbf{C}} \\ \widetilde{\mathbf{C}}\boldsymbol{\Lambda} \\ . \\ \widetilde{\mathbf{C}}\boldsymbol{\Lambda}^{f-1} \end{bmatrix} [\widetilde{\mathbf{G}} \quad \boldsymbol{\Lambda}\widetilde{\mathbf{G}} \ldots \boldsymbol{\Lambda}^{p-1}\widetilde{\mathbf{G}}] = \widetilde{\mathbf{O}}\widetilde{\mathbf{K}} \tag{39}$$

$$\text{with} \quad \widetilde{\mathbf{O}} = \begin{bmatrix} \widetilde{\mathbf{C}} \\ \widetilde{\mathbf{C}}\boldsymbol{\Lambda} \\ . \\ \widetilde{\mathbf{C}}\boldsymbol{\Lambda}^{f-1} \end{bmatrix} \quad \text{and} \quad \widetilde{\mathbf{K}} = [\widetilde{\mathbf{G}} \quad \boldsymbol{\Lambda}\widetilde{\mathbf{G}} \ldots \boldsymbol{\Lambda}^{p-1}\widetilde{\mathbf{G}}] \tag{40}$$

We note $\widetilde{\mathbf{q}}_1^o, \widetilde{\mathbf{q}}_2^o, \ldots, \widetilde{\mathbf{q}}_n^o$ the columns of the identified observability matrix $\widetilde{\mathbf{O}}$. It is easy to show that the kth column of $\widetilde{\mathbf{O}}$ is the $(mf \times 1)$ vector obtained as

$$\widetilde{\mathbf{q}}_k^o = \begin{bmatrix} \widetilde{\mathbf{c}}_k \\ \lambda_k\widetilde{\mathbf{c}}_k \\ . \\ \lambda_k^{f-1}\widetilde{\mathbf{c}}_k \end{bmatrix} \tag{41}$$

with $\widetilde{\mathbf{c}}_k(\mathrm{m} \times 1)$ being the kth column vector of the matrix $\widetilde{\mathbf{C}}$. The sequence $\left\{\widetilde{\mathbf{q}}_k^{\mathbf{O}}\right\}$ is called the identified modal time story for the kth mode obtained from the identified observability matrix. It represents the temporal contribution of the kth mode associated with the output vector $\widetilde{\mathbf{c}}_k$ to the identified observability matrix. The Hankel matrix can be decomposed by using the singular value decomposition to become

$$\mathbf{H} = \left(\mathbf{U}\boldsymbol{\Sigma}^{1/2}\boldsymbol{\Psi}\right)\left(\boldsymbol{\Psi}^{-1}\boldsymbol{\Sigma}^{1/2}\mathbf{V}^{\mathrm{T}}\right) = \overline{\mathbf{O}} \quad \overline{\mathbf{K}} \tag{42}$$

where the matrices $\overline{\mathbf{O}}(mf \times n)$ and $\overline{\mathbf{K}}(n \times mp)$ calculated from measured covariance matrices are called the measured observability and controllability matrices. By comparison we have

$$\overline{\mathbf{O}} = \mathbf{U}\boldsymbol{\Sigma}^{1/2}\boldsymbol{\Psi} = \left[\,\overline{\mathbf{q}}_1^o \quad \overline{\mathbf{q}}_2^o \ldots \overline{\mathbf{q}}_n^o\,\right] \tag{43}$$

where $\overline{\mathbf{q}}_k^o$ is the kth$(mf \times 1)$ column vector of the measured observability matrix $\overline{\mathbf{O}}$. The modal observability coherence indicator is defined as the magnitude of the normalized dot product between the vectors $\widetilde{\mathbf{q}}_k^o$ and $\overline{\mathbf{q}}_k^o$

$$\gamma_k^o = \frac{\left|\widetilde{\mathbf{q}}_k^{o*\mathrm{T}}\overline{\mathbf{q}}_k^o\right|}{\left(\left|\widetilde{\mathbf{q}}_k^{o*\mathrm{T}}\widetilde{\mathbf{q}}_k^o\right|\left|\overline{\mathbf{q}}_k^{o*\mathrm{T}}\overline{\mathbf{q}}_k^o\right|\right)^{1/2}} \tag{44}$$

Table 1 Natural frequencies and damping ratios of the simulated system

Modes	Theoretical		Identified	
	Frequency (Hz)	Damping ratio (%)	Frequency (Hz)	Damping ratio (%)
1	4.367	0.135	4.368	0.144
2	12.368	0.378	12.367	0.375
3	18.718	0.585	18.719	0.590
4	23.056	0.699	23.054	0.704

with (*T) indicating complex conjugate transposition.

In similar way we define the modal controllability coherence indicator. We note $\widetilde{\mathbf{q}}_1^c, \widetilde{\mathbf{q}}_2^c, \ldots, \widetilde{\mathbf{q}}_n^c$ the rows of the identified controllability matrix $\widetilde{\mathbf{K}}$. It is easy to show that the kth row of $\widetilde{\mathbf{K}}$ is the $(1 \times mp)$ row vector obtained as

$$\widetilde{\mathbf{q}}_k^c = \left[\widetilde{\mathbf{g}}_k \ \lambda_k \widetilde{\mathbf{g}}_k \ \lambda_k^2 \widetilde{\mathbf{g}}_k \ \ldots \ \lambda_k^{p-1} \widetilde{\mathbf{g}}_k \right] \tag{45}$$

with $\widetilde{\mathbf{g}}_k(1 \times m)$ being the kth row vector of the matrix $\widetilde{\mathbf{G}}$. The sequence $\{\widetilde{\mathbf{q}}_k^c\}$ is called the identified modal time story for the kth mode obtained from the identified controllability matrix. It represents the temporal contribution of the kth mode associated with the vector $\widetilde{\mathbf{g}}_k$ to the identified controllability matrix. The measured controllability matrix is obtained from Eq. (42)

$$\overline{\mathbf{K}} = \boldsymbol{\Psi}^{-1} \boldsymbol{\Sigma}^{1/2} \mathbf{V}^{\mathrm{T}} = \begin{bmatrix} \overline{\mathbf{q}}_1^c \\ \overline{\mathbf{q}}_2^c \\ . \\ \overline{\mathbf{q}}_n^c \end{bmatrix} \tag{46}$$

where $\overline{\mathbf{q}}_k^c$ is the kth$(1 \times mp)$ row vector of the measured controllability matrix $\overline{\mathbf{K}}$. The modal controllability coherence indicator is defined as the magnitude of the normalized dot product between the vectors $\widetilde{\mathbf{q}}_k^c$ and $\overline{\mathbf{q}}_k^c$

$$\gamma_k^c = \frac{\left| \widetilde{\mathbf{q}}_k^c \overline{\mathbf{q}}_k^{c*} \right|}{\left(\left| \widetilde{\mathbf{q}}_k^c \widetilde{\mathbf{q}}_k^{c*} \right| \left| \overline{\mathbf{q}}_k^c \overline{\mathbf{q}}_k^{c*} \right| \right)^{1/2}} \tag{47}$$

Finally, the modal coherence indicator is defined for $k = 1, 2, \ldots, n$ as $\gamma_k = \gamma_k^o \gamma_k^c$. Given a state–space model and a set of measured covariance matrices the modal coherence indicator describes the correlation between each mode of the identified state–space model and the modes directly inferred from the measured signal and thus serve as a distributed model quality measure.

6 Applications

6.1 A numerical example

Simulation studies of a four degrees of freedom (df) system, shown in Fig. 1, were carried out in order to demonstrate the validity of the theoretical background of the procedure. The input force is the combination of a random force and a harmonic force $f(t) = [\cos(60\pi t), 0, 0, 0]^{\mathrm{T}}$ acting on mass 1. The initial conditions are $x(0)=0$ and $\dot{x}(0) = 0$ where $x(t)$ is the vector displacement of masses and $\dot{x}(t)$ the vector velocity. The second-order differential equation is solved numerically with the Runge–Kutta algorithm using 1,061 samples. Only displacements of the four masses are used in the identification process. These displacements are shown in Fig. 2. The stability diagrams on eigenfrequencies and damping ratios using the modal coherence indicator are shown in Fig. 3 and the identified modal parameters together with the theoretical ones are given in Tables 1 and 2. It is observed that the natural frequencies, damping ratios and mode shapes are identified with adequate accuracy. Note that the frequency (30 Hz) and the damping ratio (0%) of the harmonic excitation can also be found from these stability diagrams. As mentioned before, the modal parameters can be estimated without measurement of the input forces. The first simulation study is carried out to illustrate this concept.

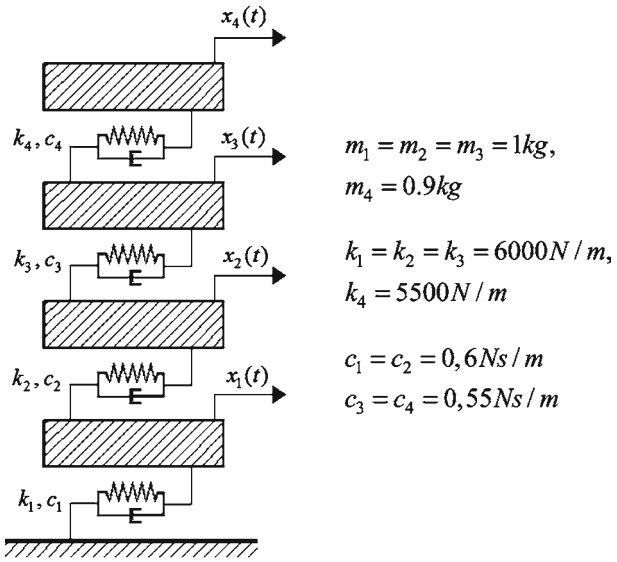

Fig. 1 Mass-damper-spring system of four degrees of freedom

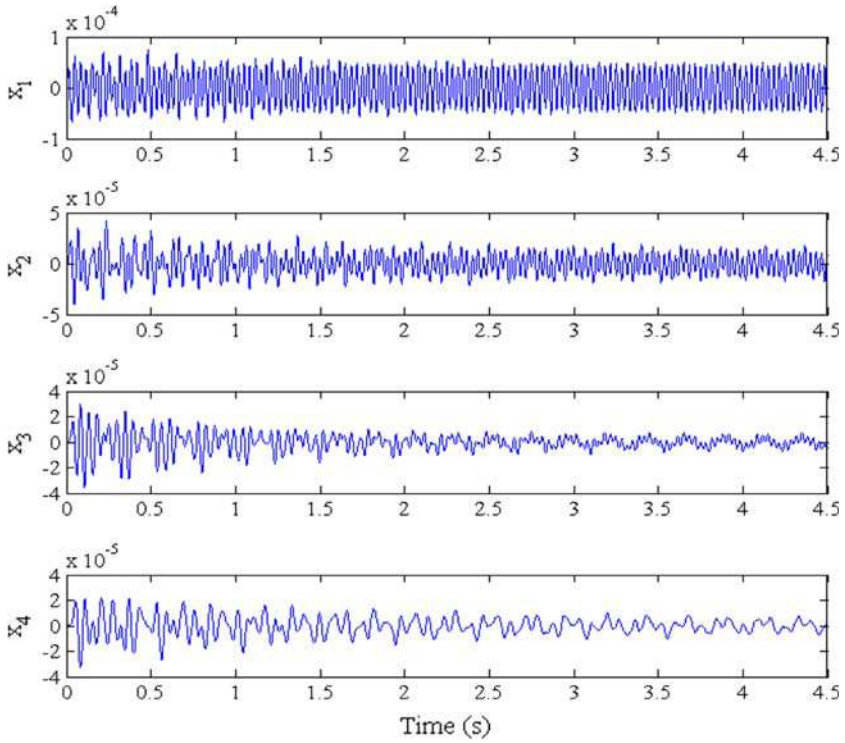

Fig. 2 Responses of the simulated system

6.2 An experimental modal analysis of a clamped beam in laboratory

The modal parameter identification procedure is now applied to a real structure in laboratory. Figure 4 shows the experimental system. It is a simple horizontal cantilever beam with five measurement locations equally spaced along the length. The mechanical characteristics of the beam are: Young's modulus $E = 2.1\,\mathrm{MPa}$, mass density $\rho = 9{,}000\,\mathrm{kg\,m^{-3}}$, moment of inertia of the beam cross-section $I = 3.8 \times 10^{-9}\,\mathrm{m^4}$, cross-sectional area $S = 485 \times 10^{-6}\,\mathrm{m^2}$ and length of the beam $L = 0.56\,\mathrm{m}$. The theoretical eigenfrequencies for the transverse vibration of the beam are obtained from the Euler–Bernoulli theory [5,25] and are given by

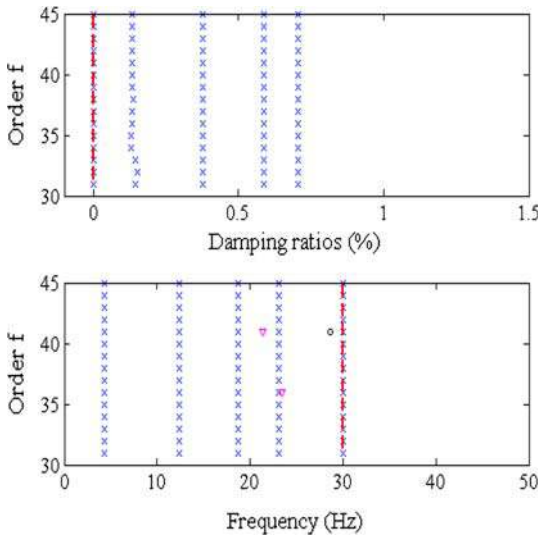

Fig. 3 Stabilization diagram on damping ratios and eigenfrequencies for the simulated system

Table 2 Mode shapes of the simulated system

	First mode	Second mode	Third mode	Fourth mode
Theoretical	$0.3489 - 0.00002$i	$-0.9118 - 0.0002$i	1	$-0.6676 - 0.0008$i
	$0.6538 - 0.00004$i	$-0.9059 - 0.0004$i	$-0.3054 + 0.00015$i	1
	$0.8768 + 0.00001$i	$0.0118 + 0.0002i$	$-0.9067 - 0.00068$i	$-0.8302 + 0.0004$i
	1	1	$0.7176 + 0.00062$i	$0.3410 + 0.00008$i
Identified	$0.3481 - 0.00003$i	$-0.9112 - 0.0003$i	1	$-0.6671 - 0.0009$i
	$0.6531 + 0.00005$i	$-0.9052 - 0.0004$i	$-0.3051 + 0.00012$i	1
	$0.8762 - 0.00001$i	$0.0114 + 0.0003$i	$-0.9062 - 0.00061$i	$-0.8309 + 0.0006$i
	1	1	$0.7179 + 0.00067$i	$0.3415 + 0.00009$i

$$f_{\chi_i} = \frac{\chi_i^2}{2\pi L^2}\sqrt{\frac{EI}{\rho S}} \tag{48}$$

For the transverse vibration of a fixed-free beam the constant values of χ_i are determined from the boundary conditions of the beam and are computed from

$$1 + \cos(\chi_i)\cosh(\chi_i) = 0 \tag{49}$$

A Gaussian random excitation is now applied transversely at the free end of the beam. The signals are sampled at the rate $\Delta t = 781.2$ μs and 8,192 data points are collected for each channel. Figure 5 shows typical output data of an accelerometer. Using only the output data of accelerometers the eigenfrequencies and damping ratios of the clamped beam are obtained from stabilization diagrams shown in Figs. 6 and 7. The state–space method and the modal coherence indicator have been applied to obtain these stabilization diagrams. The identified modal parameters together with the theoretical ones are given in Table 3. It is observed that the natural frequencies are very well identified. Finally, Fig. 8 shows the experimental mode shapes of the vibrating beam, excited with an unmeasured random input force.

6.3 An experimental modal analysis of a stay cable in laboratory

The second experimental example consists in the modal parameter identification of a line cable in laboratory. The schematic view of the testing system is shown in Fig. 9. The parameters of the cable are: mass per unit length 0.8127 kg/m, rigidity flexural (EI) 11.07 Nm^2, length of the cable 32.3 m and mechanical load 10.700 N.

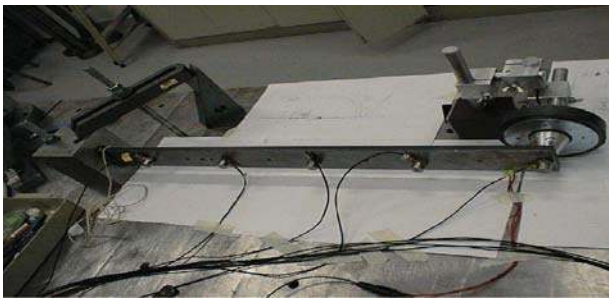

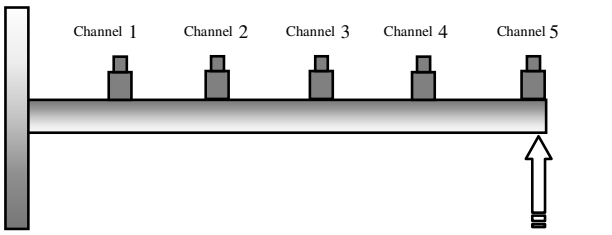

Fig. 4 Experimental procedure for the horizontal beam

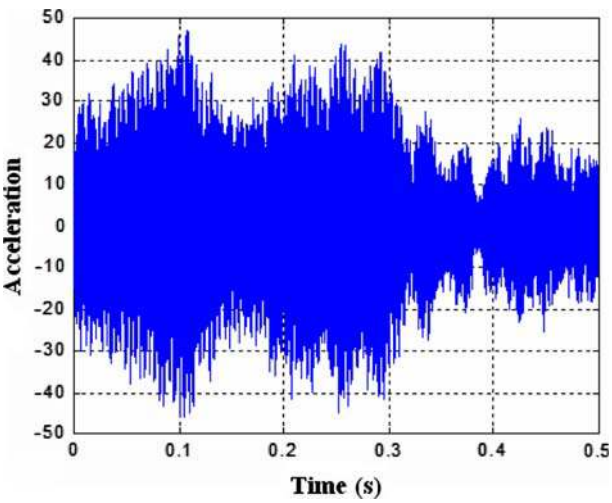

Fig. 5 Typical time response of an accelerometer

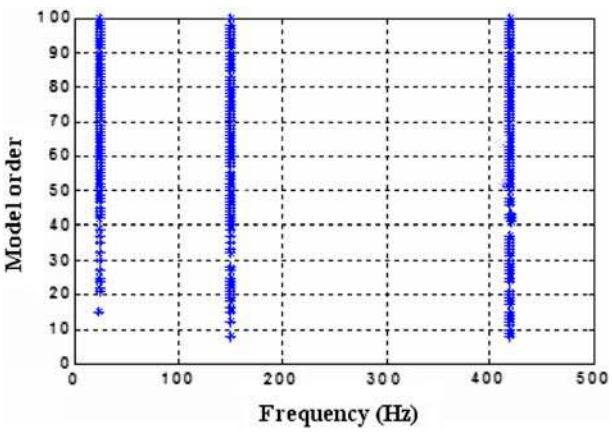

Fig. 6 Stabilization diagram on eigenfrequencies for the clamped beam

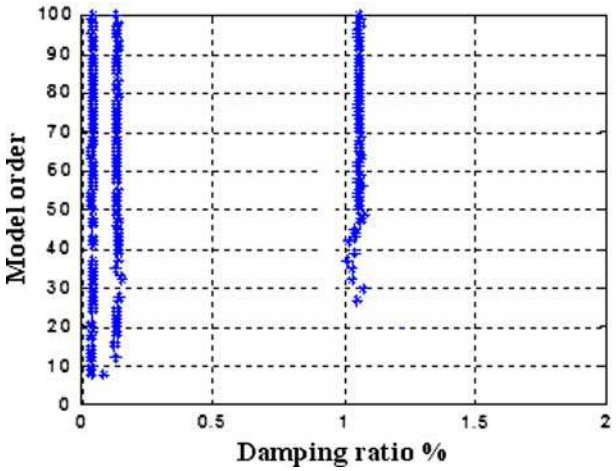

Fig. 7 Stabilization diagram on damping ratios for the clamped beam

Table 3 Natural frequencies and damping ratios of the experimental beam

Modes	Theoretical frequency (Hz)	Identified frequency (Hz)	Identified damping ratio (%)
1	24.13	24.16	1.05
2	150.81	150.58	0.13
3	422.29	423.11	0.04

These values are obtained from Barbieri et al. [26]. For the modal parameters identification four accelerometers are placed in the cable in the position L/2, 3L/8, L/4 and L/8. The excitation of the cable is obtained through an impact hammer and Fig. 10 shows the time responses of different accelerometers. Only these time responses are used to identify the modal parameters of the cable. Figure 11 shows the stabilization diagram on eigenfrequencies using the state–space method and the modal coherence indicator. This diagram shows very stable eigenfrequencies and from this plot we obtain the experimental natural frequencies of the cable. Table 4 shows the theoretical and experimental natural frequencies and damping ratios of the cable using different configurations of sensors. The theoretical natural frequencies are obtained by Rao [25]

$$f_k = \frac{\pi}{2L^2}\left(\frac{EI}{\rho S}\right)^{1/2}\left(k^4 + \frac{k^2 P L^2}{\pi^2 EI}\right)^{1/2} \tag{50}$$

where k is the free vibration mode number, L the length of the cable, P the mechanical load, S the cross-sectional area and ρ the mass density of the cable. The difference between theoretical and experimental values is justified, once the structural damping, torsion and effects of non-linearity are not present in the mathematical model which gives Eq. (50). Figure 12 shows the theoretical (solid line) and experimental (points) mode shapes of the vibrating cable. From all these results, it can be seen that good estimates of modal parameters are obtained from the state–space method, using output-only data.

6.4 An experimental modal analysis of stay cables in a cable-stayed bridge

While very sophisticated techniques have been developed in order to study the aerodynamics of bridges and stay cables, comparatively few studies have been carried out concerning the dynamic response of cable-stayed bridges. Stay cables are among the most important structural components in modern cable-stayed bridges. The cable tension plays a primordial role in the construction control and long-term monitoring of cable-stayed bridges and experimental vibration measurement is one of the most widely used methods for tension evaluation and health monitoring these cables. The state–space method is applied to the analysis of stay cables of the Jinma cable-stayed bridge (Fig. 13), that connects Guangzhou and Zhaoqing in Guangdong Province, China. It is a single tower, double row cable-stayed bridge, supported by $28\times4 = 112$ stay cables. Before the official opening of the bridge, ambient vibration tests on each stay cable were carried out for the purpose of cable

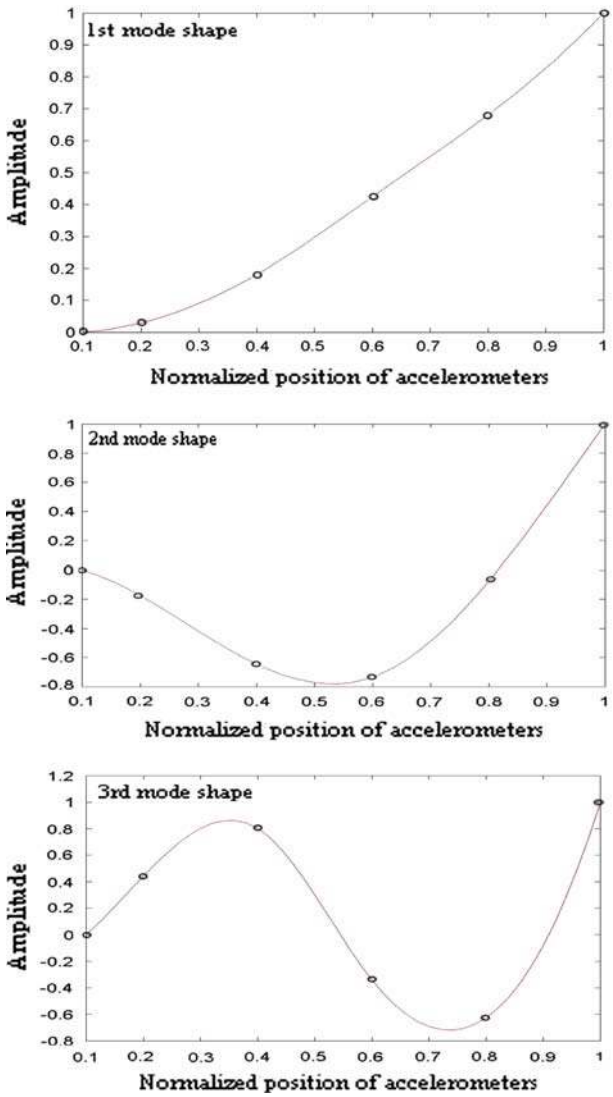

Fig. 8 The first three mode shapes of the horizontal beam

tension evaluation. Inputs could evidently not be measured, so only acceleration data are available. For the ambient vibration measurement of each stay cable an accelerometer was mounted securely to the cables, the sample frequency is 40 Hz and the recording time is 140.8 s, which results in total 5,632 data points. Cables 1, 56, 57 and 112 are the longest and cables 28, 29, 84 and 85 are the shortest. A full description of the test can be found in [27]. Figures 14 and 15 show the time response and the stabilization diagram on eigenfrequencies of cable 25. Similar results are obtained if we consider another cable. The stabilization diagram shows remarkable stable eigenfrequencies and from this plot we determine the eigenfrequencies of the cable 25. The state–space approach is applied to each of 120 stay cables to obtain the fundamental frequency f_0 of each cable. These fundamental frequencies are presented in Fig. 16. It can be seen that the fundamental frequencies of both bridge sides are almost identical and the fundamental frequency distribution is symmetric with respect to the single tower. The fundamental frequencies vary between 0.533 Hz for the longest cable and 2.703 Hz for the shortest cable. The cable tension can be estimated by the approximated expression $T = 4\mu L^2 f_0^2$ where μ is the linear density of the cable ($\mu = 66.94$ kg/m). The maximum and minimum cable forces for the Jinma bridge are then: $T_{\max} = 5.052$ kN (cable number 57), $T_{\min} = 2.490$ kN (cable number 84). These cable forces can be considered as reference tensions and used as indicators in the field of health monitoring process.

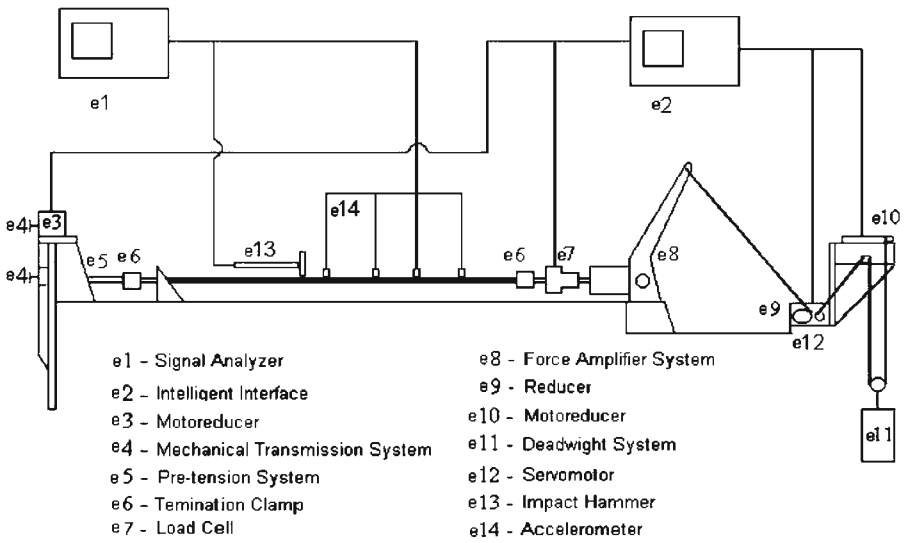

Fig. 9 Schematic view of the testing line cable

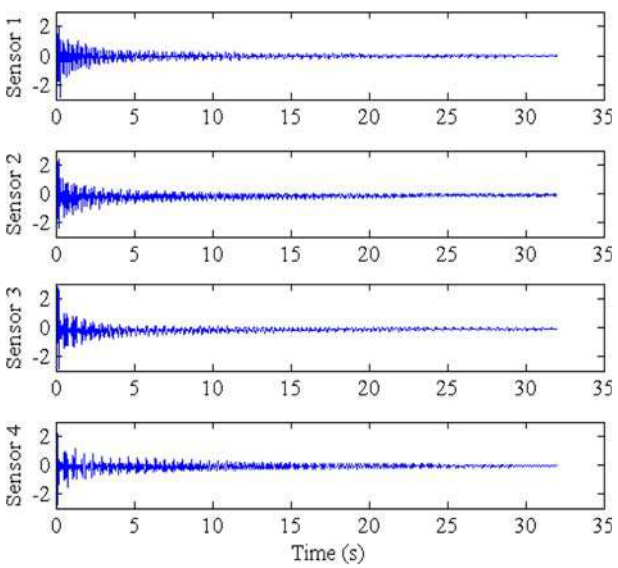

Fig. 10 Time response of accelerometers

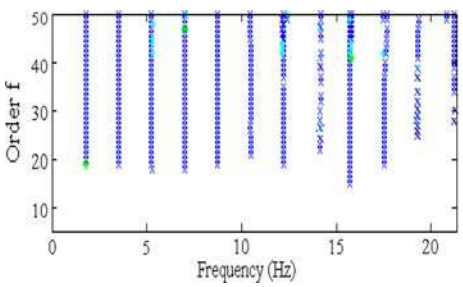

Fig. 11 Stabilization diagram on eigenfrequencies for the line cable

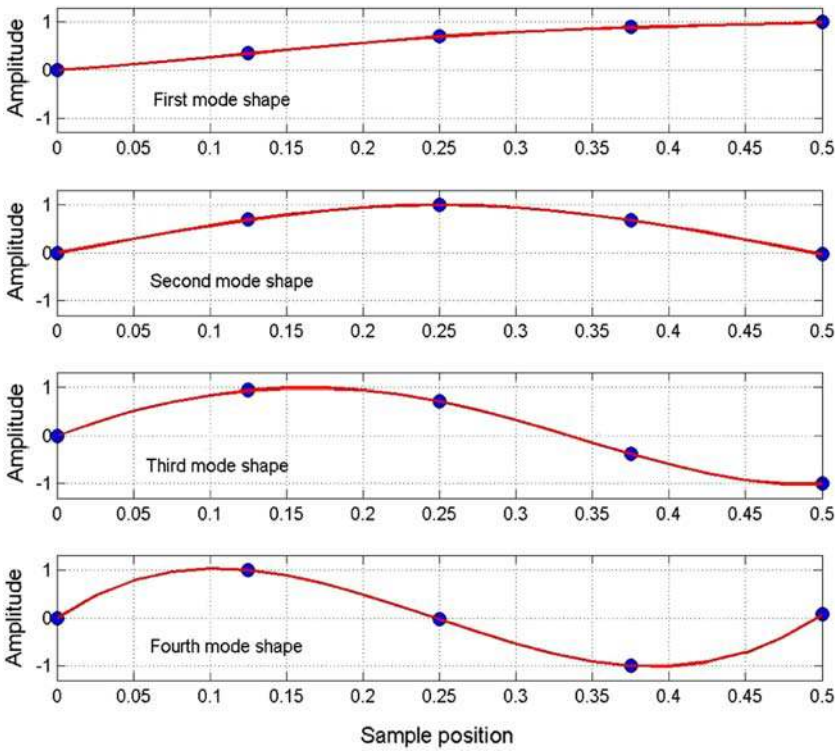

Fig. 12 Theoretical (*solid line*) and experimental (*points*) mode shapes for the line cable

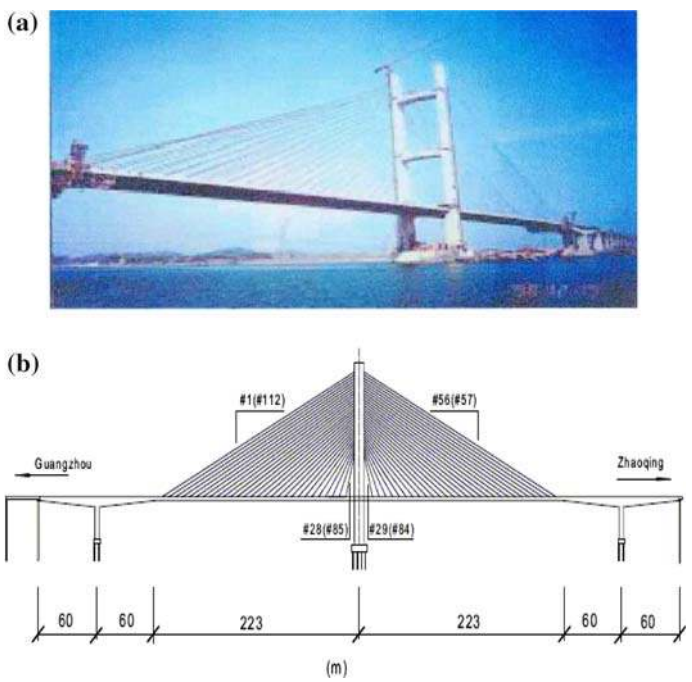

Fig. 13 **a** View of the Jinma cable-stayed bridge. **b** Schematic dawning of the bridge with stay cables

Table 4 Natural frequencies and damping ratios of the experimental cable

Modes	Theoretical frequency (Hz)	Sensor 1,2		Sensor 2		Sensor 4		Sensor 1,2,3,4	
		f(Hz)	ζ (%)	f(Hz)	ζ(%)	f(Hz)	ζ(%)	f(Hz)	ζ(%)
1	1.765	1.776	0.509	1.774	0.518	1.773	0.507	1.775	0.520
2	3.530	3.517	0.275	3.518	0.262	3.517	0.251	3.518	0.265
3	5.295	5.255	0.282	5.256	0.293	5.256	0.261	5.255	0.265
4	7.060	7.016	0.170	7.016	0.161	7.016	0.163	7.016	0.168
5	8.825	8.729	0.174	8.729	0.181	8.732	0.174	8.730	0.175

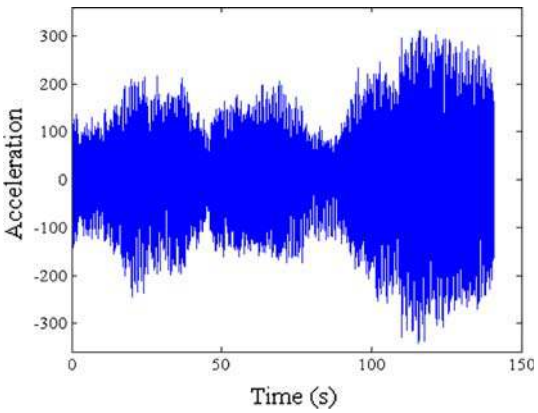

Fig. 14 Time-history response of cable 25

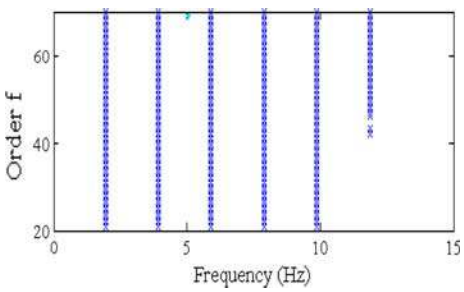

Fig. 15 Stabilization diagram on eigenfrequencies for the cable 25

7 Conclusion

In this article, we have established a simple relationship between the companion matrix and the state matrix using properties of the singular value decomposition of a block Hankel matrix. We have proved that, under full row rank condition of the block Hankel matrix, the companion matrix and the state matrix have the same eigenvalues. Consequently, the modal parameters of a vibrating system provided by the ARMAV and state–space approaches coincide. A generalized weighted concept has been analyzed, and a relationship between the eigenvectors of the state–space matrix and the eigenvectors of the companion matrix has been established. Furthermore, the properties of the ARMAV method are well known and have been thoroughly analyzed in the literature. The exact equivalence between the companion matrix and the state matrix shown in the article makes it possible to apply to the state–space model properties derived from the ARMAV approach.

We have developed a procedure for identifying modal parameters with only measured response data, and in particular we have proposed a modal coherence indicator between identified and measured modes which eliminates spurious modes. Stabilization diagrams reflect the variations of modal parameters with the row increments of the block Hankel matrix. These diagrams are combined with the modal coherence indicator to isolate the structural modes and to eliminate the unwanted computational modes. It is shown that the state–space method can be effectively employed in operational modal analysis, and this output-only measurement

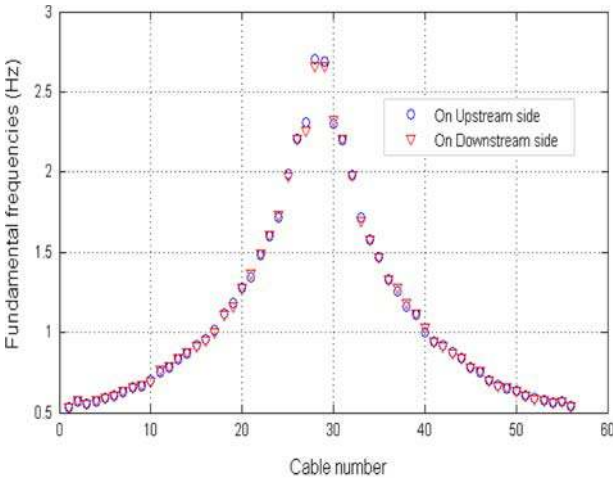

Fig. 16 Fundamental frequency of each cable on upstream side and on downstream side

technique has already demonstrated its robustness and reliability when applied to ambient vibrations, especially in modal parameter identification of stay cables. Operational modal analysis applied to the dynamic data of stay cables provides useful information to determine the current condition of stay cables accurately.

Large structures tend to present large motions, and therefore nonlinearities. The use of the state–space approach for the identification of nonlinearities on damping and stiffness is under investigation.

Acknowledgments The authors would like to thank Dr. Barbieri at the Pontificia Universidade Catolica do Parana (Brazil) and Dr. Ren at the University of Fuzhou (Republic of China) for generously providing the data for this study.

References

1. Ljung, L.: System Identification-Theory for the User. Prentice-Hall, Englewood Cliffs (1987)
2. Juang, J.N.: Applied System Identification. Prentice-Hall, Englewood Cliffs (1994)
3. Pandit, S.M., Wu, S.M.: Time Series and System Analysis with Applications. Wiley, New York (1983)
4. Pandit, S.M.: Modal and Spectrum Analysis: Data Dependent Systems in State Space. Wiley, New York (1991)
5. Harris, C.M.: Shock and Vibration Handbook. Mc-Graw Hill, New York (1996)
6. Papagiannopoulos, G.A., Beskos, D.E.: On a modal damping identification model of building structures. Arch. Appl. Mech. **76**, 443–463 (2006)
7. Kompalka, S.A., Reese, S., Bruhns, O.T.: Experimental investigation of damage evolution by data-driven stochastic subspace identification and iterative finite element model updating. Arch. Appl. Mech. **77**, 559–573 (2007)
8. Lardies, J.: State space identification of vibrating systems from multi output measurements. Mech. Syst. Signal Process **12**, 543–558 (1998)
9. Van Overschee, P., De Moor, B.: Subspace identification for linear systems: theory implementation and applications. Kluwer, Dordrecht (1996)
10. Pi, Y.L., Mickleborough, N.C.: Modal identification of a vibrating structure in the time-domain. Comput. Struct. **32**, 1105–1115 (1989)
11. Lardiès, J., Ta, M.N., Berthillier, M.: Modal parameter estimation based on the wavelet transform of output data. Arch. Appl. Mech. **73**, 718–733 (2004)
12. Ruzzene, M., Fasana, A., Garibaldi, L., Piombo, B.: Natural frequencies and damping identification using the wavelet transform: application to real data. Mech. Syst. Signal Process **11**, 207–218 (1997)
13. Ibrahim, S.R.: Random decrement technique for modal identification structures. J. Spacecr. Rockets **14**, 696–700 (1977)
14. Petsounis, K.A., Fassois, S.D.: Parametric time-domain methods for the identification of vibrating structures-critical comparison and assessment. Mech. Syst. Signal Process **15**, 1031–1060 (2001)
15. Zhang, Y., Zhang, Z., Xu, X., Hua, H.: Modal parameter identification using response data only. J. Sound Vib. **282**, 367–380 (2005)
16. Peeters, B., De Roeck, G.: Stochastic system identification for operational modal analysis: a review. J. Dyn. Syst. Meas. Control **123**, 659–667 (2001)
17. Hermans, L., Van Der Auweraer, H.: Modal testing of structures under operational conditions: industrial applications. Mech. Syst. and Signal Process **13**, 193–216 (1999)
18. Mevel, L., Basseville, M., Goursat, M.: Stochastic subspace-based structural identification and damage detection—application to the steel quake benchmark. Mech. Syst. Signal Process **17**, 91–101 (2003)
19. Huang, C.S.: Structural identification from ambient vibration measurements using the multivariate AR model. J. Sound Vib. **241**, 337–359 (2001)

20. Garibaldi, L., Giorcelli, E. Piombo B.: ARMAV techniques for traffic excited bridges. J. Vib. Acoust. **120**, 713–718 (1998)
21. Pi, Y.L., Mickleborough, N.C.: Modal identification of vibrating structures using ARMA model. J. Eng. Mech. **115**, 2232–2250 (1989)
22. Lenzen, A., Walter, H.: Damage detection by system identification. An application of the generalized singular value decomposition. Arch. Appl. Mech. **66**, 555–568 (1996)
23. Aoki, M.: State Space Modeling of Time Series. Springer, Berlin (1990)
24. Viberg, M.: Subspace-based methods for the identification of linear-time invariant systems. Automatica **31**, 1835–1851 (1995)
25. Rao, S.: Mechanical Vibrations. Addison-Wesley, Reading (1995)
26. Barbieri, N., Honorato de Souza Junior, O., Barbieri, R.: Dynamical analysis of transmission line cables. Linear Theory. Mech. Syst. Signal Process **15**, 1031–1060 (2001)
27. Ren, W.X., Chen, G.: Experimental modal analysis of stay cables in cable-stayed bridges. In: Proceedings of the 21th IMAC, Kissimmee, Florida (2003)